

Abstract

Effective strain in composites as well as potential rupture and debonding of composite materials play a crucial role in predicting the strength of retrofitted reinforced concrete (RC) beams. However, only limited experimental data on these phenomena is available, mainly due to the inadequacy of traditional monitoring systems. This paper presents a comparative analysis of different instrumentation for monitoring retrofitted RC elements. In particular, the paper addresses beams retrofitted with composite materials (FRP and FRCM) and considers strain gauges (SG), fibre-optic Bragg grating (FBG) sensors, linear variable differential transformer (LVDT), digital image correlation (DIC) and acoustic emission (AE) sensors for monitoring strain, displacement, cracking and debonding. Experiments on six beams were carried out and the measured data from the monitoring devices was compared. The accuracy of DIC for strain and displacement monitoring, as well as the ability of using AE for detecting cracks and debonding, were shown to match the performance of traditional methods, with the added benefit of providing full-field and depth monitoring. This is of particular interest for composite-strengthened concrete elements in which the accurate measurements of effective strain and debonding of the composite material can lead to developing more precise design formulae.

Keywords

A. Carbon Fiber; D. Acoustic Emission; D. Non-destructive testing; Digital Image Correlation (DIC)

1. INTRODUCTION

The external retrofit of RC beams with fibre reinforced polymer (FRP) sheets is a well-studied area of research and in particular for monotonic loading, a large number of experimental campaigns has been carried out (e.g. Barros et al., 2007; El-Ghandour, 2011; Esfahani et al., 2007). Compared to other traditional retrofit techniques, FRP retrofits have the benefit of extended durability, no corrosion and reduced labour time, while enhancing the flexural or shear capacities of members without increasing their weight or stiffness (Bousselham, 2010). There is

already a wealth of design guidelines for the shear and flexural strengthening of beams with FRP, such as the American ACI-440.2R-08 (ACI 440, 2008), the Canadian CSA-S806 (CSA, 2012), the fib Bulletin 14 (fib, 2001) and the Italian CNR-DT-200 (CNR, 2012).

The use of textile reinforced cementitious mortar jackets (TRCM) for strengthening beams, consisting of composites within a cement matrix, has some benefits over FRP retrofits including fire resistance and (Verbruggen et al., 2014). However, only little experimental data is available and currently no guidelines are available to inform potential retrofit designs (Babaeidarabad et al., 2014).

A topic of particular importance studied in recent years is the evaluation of effective strain in external composite strengthening materials. The measure of effective strain is used by most guidelines to predict the contribution of FRP to shear strength and flexural capacity of strengthened elements in particular. It is also an important parameter when determining FRP to concrete bond and anchorage. An important number of recent research efforts focus on determining experimental values of effective strain in FRP sheets and comparing it to values determined by code equations (e.g. Lee et al., 2012; Lu et al., 2009; Sayed et al., 2014; Teo and Yin, 2014). A previous study assessing the major design guidelines for the seismic retrofit of RC beam-column joints with FRP has also highlighted the assessment of effective FRP strain as a crucial factor in the ability of design guidelines to predict accurate values of shear strength enhancement (Pohoryles and Rossetto, 2014). In essence, most design guidelines currently suggest the use of low design and effective strains, which are below the maximum bond strain limits. For instance, a limit of 0.4% strain is recommended by the CNR guidelines (CNR, 2012), which seems overly conservative according to experimental results presented in the literature (Bisby and Stratford, 2011; Del Vecchio *et al.*, 2014). It is hence of great importance to gather more data on experimental strains recorded on the FRP surface. .

To obtain effective strain values experimentally, an important aspect is the instrumentation chosen to measure strain. In the literature, several ways in which strains on material surfaces can be measured, are reported. Most studies usually employ traditional monitoring systems for strain measurements on the retrofit surface, if measured at all, consisting of strain gauges. Hence, they provide only punctual measurements (e.g.: Mazzotti et al., 2009). Other methods such as fibre-optic sensors can provide measurements at multiple points, but still only along the

line of the fibres. FBG sensors are commonly used in structural health monitoring applications, as they are able to monitor large distances and are small and durable. While strain gauges are based on measuring changes in electrical resistance upon deformation of the gauge, for FBG sensors, strain is derived from changes in light wavelength reflected from Bragg gratings, which deform as the material strains, resulting in a small change in the spatial period (Kaiser and Karbhari, 2004). Strain can be measured at multiple locations using a method called multiplexing, analysing changes in different frequencies of light. In a past study on FRP strengthened beams, the strain measurements of FBG sensors were observed to be sensitive to changes in the installation of the sensors and in particular to the thickness of the adhesive used (Lau et al., 2001). Proper installation and surface preparation are essential to ensure reliable measurements (Zhang et al., 2003).

There is a clear need to determine the effective strain reached in FRP fibres across the entire strengthening in order to provide information on whether current guidelines are too conservative. Hence other measurement techniques are required. In this paper, digital image correlation (DIC), an optical, non-destructive and non-contact strain measurement technique, which provides full-field measurements of strain, is explored as a possible measurement technique for this purpose. Using DIC, one can obtain strain or displacement fields on the surface by comparing local correlation between two images before and after deformation. DIC software looks for observable changes in the images to derive a deformation field describing the displacement taking place in the sample. Using two or more cameras (stereoscopic view) it is possible to measure 3D deformation fields (Goideanu et al., 2013). Compared to photogrammetry, which usually implies the use of reflective targets on the surface of the specimen, in DIC, natural patterns of materials or man-made patterns, such as speckled paint, can be used (Pan et al., 2008). This reduces the work needed to apply targets, but importantly provides the main advantage compared to strain gauges or fibre optics, as it is possible to measure strain continuously over the entire area of interest, rather than at single points.

A short survey of available literature indicates that only few studies exist that use DIC to evaluate strain in FRP strengthened RC elements. These however often concentrate on small samples such as shear debonding tests of FRP from concrete blocks in tensile tests monitored with 2-D DIC (e.g.: Ali-Ahmad et al., 2006; Corr et al., 2007). Work by Bisby and Stratford

(2011) on FRP confined concrete cylinders shows a local variation of FRP strains, which can practically only be measured by DIC, and show that the effective strains of FRP may be closer to their ultimate values than previously assumed. These studies serve as proof-of-concept for this experimental measurement and data acquisition technique as they have generally shown good results.

For full RC members, tests on beams strengthened in flexure by FRP are presented in Kurtz *et al.* (2008) and show a good match between strain gauge data and DIC. Attari *et al.* (2012) also use DIC to assess FRP strains and deflections in flexurally strengthened FRP beams and obtain a good qualitative match to data recorded with strain gauges and LVDT's, however no quantitative comparison of data is presented. Verbruggen *et al.* (2014) used DIC to record strains and cracks in FRP and TRCM strengthened beams, but no comparison to traditional methods is offered. Finally, Lee *et al.* (2010) employ DIC to measure strain fields in cyclic tests on beam-column joints strengthened with FRP. In particular, the ease of using DIC and accuracy of results are pointed out by the authors.

Next to effective strain, it is important to monitor potential failure mechanisms such as debonding, fibre-rupture or end peeling of concrete and cracking of concrete beneath the composite retrofit jackets. This is rarely monitored using instrumentation, but rather by visual inspection (e.g. Akguzel and Pampanin, 2010). In this case, acoustic emission (AE) monitoring may offer more insight, as it enables to discriminate among different sources of damage, thereby attributing each emission to a particular source type or failure mode (Degala *et al.*, 2009). AE monitoring is a commonly used form of passive, non-destructive testing (NDT) that has been in use for nearly 50 years (Dunegan and Harris, 1969). Acoustic emissions are elastic waves spanning a range of frequencies emitted as a material is stressed and deformed. These acoustic pulses are transmitted through the sample and recorded using piezoelectric transducers, which convert the mechanical energy of the wave to electrical signal (Grosse *et al.*, 2003). AE testing is considered very useful in detecting defect processes as they are occurring during loading and in a wide range of materials. The AE monitoring of cracks in concrete structures for assessing their need for maintenance or retrofit is not uncommon (Ohtsu, 2008) and codes of practice such as the JCMS-III (2003) are in place to establish the recommended practice. Different debonding mechanisms and fractures in different materials emit acoustic

signals with different characteristics, and this can be exploited to monitor debonding of the composite strengthening jackets and cracking below them far before visual detection is possible (Wevers, 1997).

While different monitoring techniques have already been evaluated for monitoring damage in simple, FRP samples (e.g.: Goidescu et al., 2013), this paper aims to comparatively evaluate techniques of monitoring experiments on composite strengthened RC beams. The focus lies on the measurement of effective strain and debonding, which have been highlighted as factors of crucial importance in enhancing the current state of retrofit guidelines. The objectives of this study is to compare accuracy in measuring strain and displacement using different sensors, but also to assess ways of measuring FRP and FRCM debonding or rupture. To this purpose an experimental study on six 1/3 scaled beams retrofitted with FRP and FRCM is conducted. Five different monitoring techniques are used and compared in two positions of the beams. Electrical strain gauges (SG), fibre-optic Bragg grating (FBG) sensors and DIC are used to monitor strain on the concrete or FRP surface, AE sensors are used to assess debonding mechanisms of the FRP and linear variable differential transformers (LVDT) are used to measure vertical deflection of the beam.

2. EXPERIMENTAL SETUP AND PROCEDURE FOR DATA COLLECTION

2.1. SET-UP

Six T-beam specimens were tested under monotonic loading in a four-point bending instrument with the specimen geometry shown in Figure 1. The reinforcement detailing and geometry were the same for all specimens.

For three beams FRP was applied for flexural strengthening to the bottom face of the beam and as U-strips for anchorage and shear strengthening. As shown in Figure 1, the retrofit consisted of one or two layers of 80mm wide FRP sheet placed along the bottom face of the beam. The ACI 440.2R-08 guidelines were followed to determine the transversal anchorage area required for bottom longitudinal sheets. For beam FRP1-a with one layer of FRP, three 4cm U-strips with 140mm separation were used for shear strengthening and anchorage, while for beam FRP2 with two layers of bottom FRP, a full U-wrap along the length requiring anchorage was provided.

For the two beams with fabric-reinforced cementitious matrix (FRCM1 and FRCM2) strengthening 1 or 2 layers were applied as a U-wrap along the length of the beam.

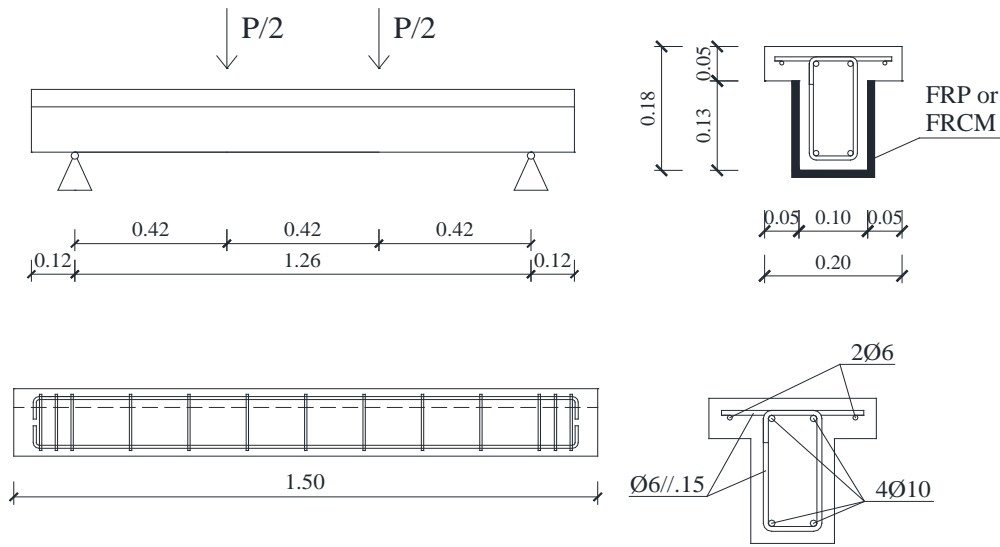


Figure 1 - Beam specimens tested at the UCL concrete lab (dimensions in meters)

A summary of the tested specimens, the instrumentation used for each test and concrete compressive strength from three standard cube 150x150x150mm³ tests (f_{cu}) can be found in Table 1. The steel reinforcement used consisted of 10mm longitudinal bars ($f_y = 550$ MPa) and 6mm smooth transverse bars ($f_y = 400$ MPa).

Table 1. Summary of beam tests – materials and instrumentation

#	Strengthening	f_{cu} (MPa)	SG	FBG	DIC	AE
C	control	30.7	X		X	
FRP1-a	FRP - 1 layer	30.1	X		X	
FRP1-b	FRP – 1 layer	25.0	X	X	X	X
FRP2	FRP - 2 layers	24.8	X	X	X	X
FRCM1	FRCM – 1 layer	29.0	X	X	X	X
FRCM2	FRCM – 2 layers	25.0	X	X	X	X

SG – strain gauge; FBG – fibre-optic sensor; DIC – digital image correlation; AE - acoustic emission sensor

The main properties of the composite materials used are found in Table 2. The unidirectional CFRP sheets used in this experiment were S&P C-Sheet provided by S&P reinforcement. The epoxy resin to apply the CFRP sheets was the recommended S&P resin 55. The FRP composite was applied to the surface of the concrete specimen using the wet-layup procedure

recommended by the manufacturer. For the specimens strengthened with FRCM, S&P ARMO-mesh 200//200 and S&P ARMO-crete w from S&P reinforcement were used. The mortar S&P ARMO-crete w was applied according the manufacturer's recommendations on clean and wet beam surfaces.

Table 2. Material properties of CFRP sheets and carbon mesh (for FRCM) used as stated in technical data sheets

	Fibre weight [g/m ²]	Elastic modulus [kN/mm ²]	Tensile strength [N/mm ²]	Rupture strain [%]	Thickness [mm]
S&P C-sheet 240	400	> 240	> 4300	1.7	0.223
S&P ARMO-mesh 200/200	2 x 80	240	4000 - 4800	1.5 - 2.0	0.044

2.2. INSTRUMENTATION

The full test set-up is shown in Figure 2. The four-point bending testing rig, load cell, as well as the monitoring set-up are shown. The tests are force controlled and the load is applied linearly up to failure of the beam with a rate of 0.2kN/s using a 300kN AEP TC4 load cell.



Figure 2 - Full beam test set-up with DIC cameras

The monitoring set-up shown in Figure 3 consists of three Linear Variable Differential Transformers (LVDTs) for measuring displacements in zone A at mid-span (50mm stroke) and the locations of applied load, zone C (25mm stroke), the integrated load sensor of the load cell, two cameras used for DIC, three strain gauges placed on the concrete surface, up to six FBG sensors placed on the concrete and FRP surfaces and two AE sensors placed on different faces of the beam.

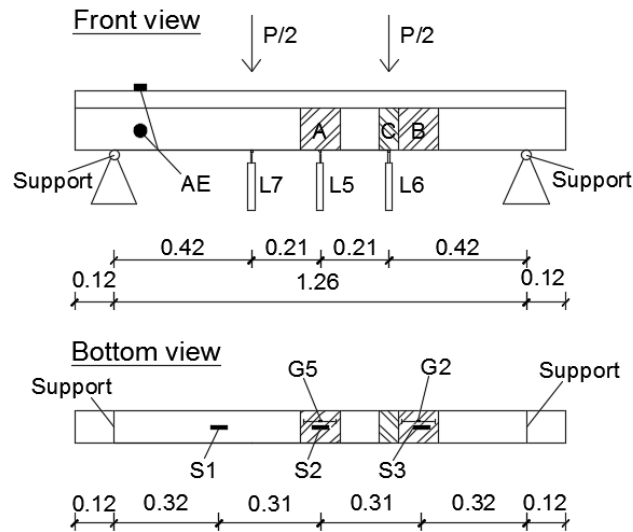


Figure 3 - Location of different sensors (G - Fibre-optic Bragg Grating; L - LVDT; S - Strain Gauge; AE and zones A, B and C for DIC)

As shown in Figure 3, the cameras for DIC are placed at 750mm at an angle of 45° to the side face of the beam. The investigated surface was painted with a high contrast random speckle pattern (Figure 3) in order to obtain more accurate strain readings. The specimens are also illuminated using a strip of LEDs to provide uniform light intensity across the surface. Two IDS 5MP sensors equipped with 8mm focal length lenses with an angle of view of 45° are used. The pixel size of the sensors is $2.2\mu\text{m}$. In order to acquire pictures from both cameras simultaneously at set intervals of 1Hz, the VMSCapture software developed by Prof. Stuart Robson from the UCL Civil, Environmental and Geomatic Engineering department is used. The DIC analysis is performed using LaVision DaVis 8.2.1.

Strain gauges and fibre-optics are placed parallel to each other along the beam bottom face. Three strain gauges are placed at the centre of the beam and below the locations of applied load. The strain gauges used in the experiments are foil gauges by Micro-measurements with $\pm 0.6\%$ accuracy. The fibre-optics are produced at City University London. The FBG sensors used are 500 mm long and are placed along the length of the beam with 5 Bragg gratings spaced at 100 mm. The Bragg gratings of the FBG sensors are aligned with the centres of the strain gauges, as shown in Figure 4. During four of the beam tests, two PZT-5H compressional crystal sensors (500kHz resonant frequency) were placed on the specimens in order to record

acoustic emissions in a range up to 1000kHz using a multi-channel Vallen AMSY-5 AE recording system. The signal was pre-amplified by a gain of 40dB.

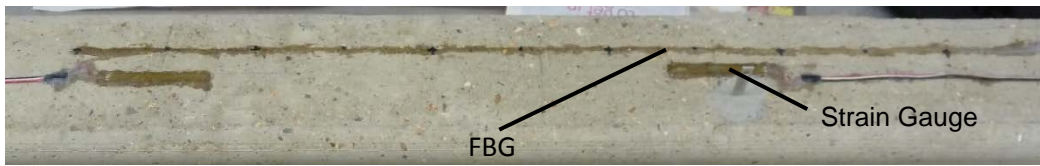


Figure 4 - Fibre-optics and strain gauge set-up on bottom beam face

3. METHODOLOGY

For the comparative analysis of the sensors, data collected with electric strain gauges is used as a baseline for comparison with the other techniques, as it is the most generally adopted means of strain measurement. Similarly, displacement recorded using LVDT's is taken as the accepted baseline for comparison.

For strain and displacement calculations in the DIC analysis, several parameters need to be chosen that can affect the data collection. The calculation speed was set to accurate rather than fast and the subset size for analysis was recommended to be 31 by 31 pixel large with a 9 pixel step size (about 1/3 of the subset size). To obtain strain data comparable to the SG and FBG data, the "virtual strain gauge" function in DaVis is used. This allows the measurement of strains along the same length as the length of the SG. For the control and FRP strengthened beams, reasonable comparisons between strains recorded on the bottom surface by SG and FBG sensors, as well as by DIC on the bottom of the side face of the beam can be made. For FRCM strengthened beams FRCM1 and FRCM2, the DIC "virtual strain gauge" is placed at the side face of the beam at the same height as the underside of the concrete beam, in the same position as the SG and FBG sensors. The data for the different monitoring systems is recorded at different sampling frequencies and all the data is adjusted to the lowest sampling frequency of 1Hz is chosen for data comparison.

The objective of the AE measurements was to characterise different types of damage in the specimens, as well as identifying which materials are the source of the AE signal. Next to the main parameters such as amplitude of events and accumulated count of hits, the two following factors were hence analysed.

The parametric analysis of RA and Af values is suggested by the Japanese JCMS guidelines (JCMS III, 2003) to be used to classify different types of cracking mechanisms. RA corresponds to the ratio of rise time (ms) against amplitude (V) of hits and Af is the average frequency of events, i.e. the count of hits against the rise time for each record. A high Af to RA ratio can be related to hits caused by tensile cracks, while a low ratio is related to shear movement cracks. According to the guidelines, the limiting ratio to identify the crack type is defined by the slope of the average values of both parameters for at least 50 hits. The application of this analysis has been used to categorise cracks in RC beams (Ohno and Ohtsu, 2010; Shahidan et al., 2013), however only limited evidence for the application of this analysis for FRP or FRCM strengthened beams can be found (Verbruggen et al., 2014).

Different material damage processes lead to AE hits with different transient wave forms, and transient frequency of a hit can hence be related to different material fracture or debonding mechanisms (Gutkin et al., 2011). Frequency contents of AE events recorded for RC beams under three-point bending were reported to be around 100-200kHz (Maji and Sahu, 1994) for concrete cracking. Previous studies on frequency contents for FRP in strengthened RC elements have been reported by Gutkin et al. (2011) and Degala et al. (2009). Debonding, fibre-pull-out and fibre rupture can be identified as separate events, emitting signals with different frequency content. The frequency ranges reported are however specific to the type of FRP and the fibre density, to identify the transient frequencies of AE hits for the materials used in this study, tests on material samples were hence carried out. For concrete, a cube test was carried out and for FRP, a shear debonding test was carried out. The latter was used in particular to identify the FRP-to-concrete debonding transient frequencies. For concrete, frequencies between 100 and 175 kHz were recorded, which is in line with literature. For the shear debonding, three distinct clusters of frequency ranges were observed. The lowest range, again between 100 and 175 kHz, was attributed to concrete cracks, while the ranges 300 to 420 and 700 to 900 kHz were attributed to rupture of individual FRP fibres and FRP debonding respectively.

4. RESULTS AND DISCUSSION

4.1. COMPARISON OF STRAIN MEASUREMENTS

In order to compare the three approaches for strain measurement, the results at two different locations, zone A and B (Figure 3), are analysed. For all beams, reasonable comparisons between strains recorded on the bottom surface by strain gauge and fibre-optics, as well as by DIC on the bottom of the side face of the beam is made. For specimens C and FRP1-a, no fibre-optics are applied, and DIC is compared to strain gauges only. For beam FRCM2, only strain gauge and fibre-optic data on the concrete surface can be compared as the thickness of two layers of FRCM proves too large for reasonable comparisons to DIC. For beam FRP1-a it is not possible to make an adequate comparison for zone B as half of the concrete strain gauge is placed below a transversal FRP strip, and relative strains between concrete and FRP strip are hence recorded instead of the concrete surface.

To compare the strains, the ratio of FBG and DIC strains to SG strains are taken. The mean value of the ratio over all recorded data points, as well as the standard deviation are used to assess the accuracy of the sensors. A two-sample unequal variance t-test is also performed to test the significance of any differences between the strain measurements. Plots of strain evolution with time measured using the three sensors for beam FRP2 and FRCM1 are shown in Figure 5. The match of the three monitoring techniques shows near perfect agreement for some beams (FRP2), but less for others (FRCM1).

Table 3. Comparison of measured strains for the three sensors

	beam zone	C		FRP1-a		FRP1-b		FRP2		FRCM1		FRCM2		mean
		A	B	A	A	B	A	B	A	B	A	B		
DIC	ratio	1.20	1.13	1.05	0.99	1.02	1.09	0.98	0.96	0.95	/	/		1.04
	s.d.	0.11	0.54	0.11	0.20	0.22	0.07	0.08	0.62	0.55	/	/		0.30
	t-test	8%	91%	19%	65%	39%	63%	99%	90%	39%	/	/		
FBG	ratio	/	/	/	1.45	1.29	1.50	0.85	1.24	1.29	1.50	1.25		1.29
	s.d.	/	/	/	0.14	0.09	0.49	0.22	0.28	0.07	0.26	0.20		0.22
	t-test	/	/	/	0%	0%	15%	81%	86%	2%	1%	0%		

The results from all beams at the two measurement locations (zone A and B) is reported in Table 3. Overall it can be observed that DIC gives very close results to the SG data, with an average ratio of strains of 1.04, while the difference of the FBG sensors is higher, with a ratio of 1.29. The higher average standard deviation for the DIC data (s.d. = 0.30), however indicates more variance within the data as compared to the FBG sensors (s.d. = 0.22). For the t-test,

values lower than $p=0.05$ indicate a significant difference between the means of two data series. It can be seen that the results are not significantly different for all nine measurement series for the DIC, while the difference is significant in five out eight tests for the FBG sensors.

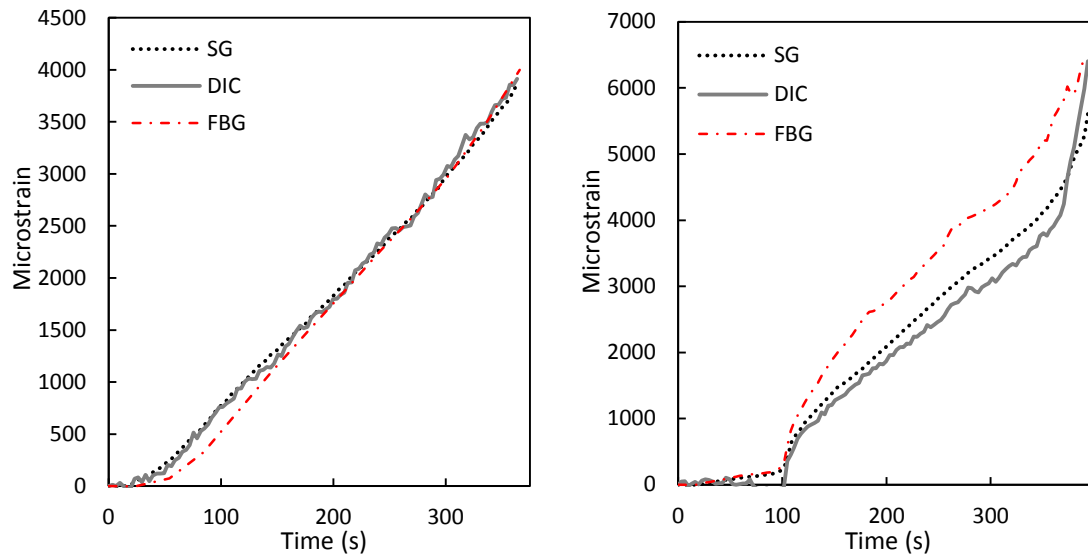


Figure 5 - Comparison of measurements from the three sensors for beam FRP2 (left) and FRCM1 (right) in zone B

The significant difference between SG and FBG strain measurements is likely to be related to an imperfect surface preparation or application of the FBG sensors, highlighting another benefit of DIC, which is not sensitive to the surface of the specimen. Moreover, from Figure 5, it is observed that for the three beams (FRP 1-b, FRCM1 and FRCM2) with significant differences between FBG and SG measurements, the FBG data only begins to significantly vary above strain values around $1000\mu\text{s}$. The measurements are therefore also compared for values below $1000\mu\text{s}$ only and, as shown in Table 4, in this case the average ratio (1.16) and the standard deviation (0.20) are lower. When limiting the analysis range, the difference is only significant for one measurement point (FRCM2 zone A). It is likely that at higher levels of strains, the difference between the two "contact" monitoring techniques increases due to the formation of cracks. These affect the longer FBG sensors more, as cracks anywhere along the entire length of the fibre can affect the reading at the two Bragg gratings of interest, while the SG and DIC readings would only be affected by cracks at the location of interest. For the same reason, when

proximity of cracks to the locations of the strain gauges is observed, the obtained results from DIC are particularly sensitive to the correct placement of the virtual strain gauge.

Table 4. Comparison of FBG and SG measurements for strain values below 1000 μ s

beam	FRP1-b		FRCM1		FRCM2		mean
zone	A	B	A	B	A	B	
ratio	1.16	1.14	0.73	1.28	1.54	1.13	1.16
s.d.	0.09	0.11	0.46	0.11	0.33	0.09	0.20
t-test	44%	33%	50%	38%	1%	31%	

It is shown that DIC gives very accurate strain readings that are independent of surface preparation and hence more reliable than traditional “contact” measurement techniques. The clear advantage of DIC over traditional techniques is however the capability of full-field strain measurements as shown in Figure 6. It is observed that, the location of cracks are easily visualised in terms of local maxima in strain. By means of full-field DIC analysis, crack locations can be anticipated before they are visible to the naked eye. DIC is hence not only very useful for strain measurements but also monitoring the formation of cracks. This is a significant improvement compared to using strain gauges on the one hand and for localising and recording cracks manually on the other hand.

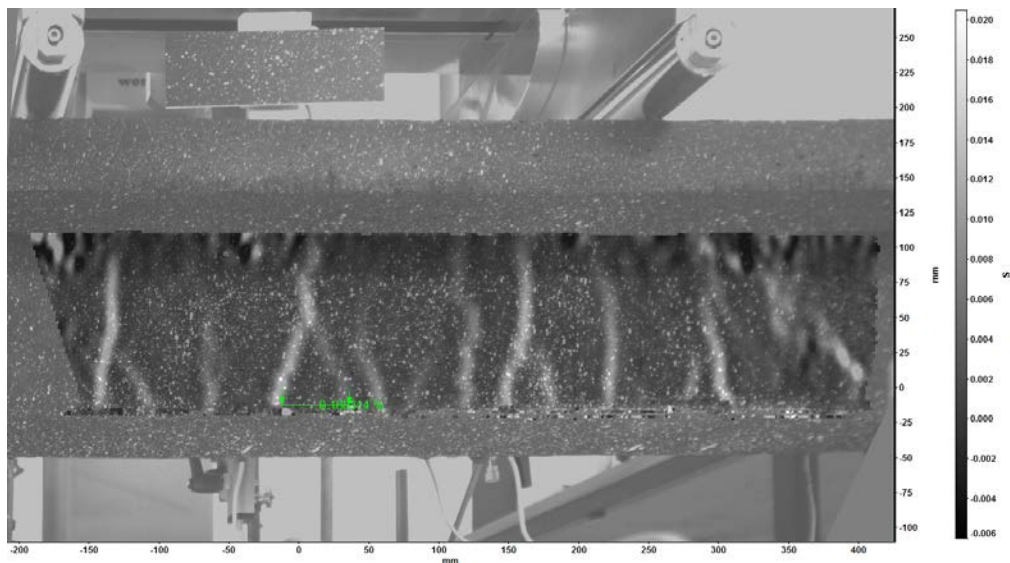


Figure 6 - Strain field measurement and virtual strain gauge for beam FRP1-a as analysed with DaVis

4.2. COMPARISON OF DISPLACEMENT MEASUREMENTS

Vertical deflection was also compared at two monitoring locations, zone A and C. In order not to be in the field of vision and affect the DIC analysis, the LVDTs are placed at the back side of the beams, while the measurement with DIC was performed at the front side of the beam.

Deflection was measured from the underside of the flange of the t-beams for both sensors.

Again, next to a ratio of measured displacement values, the standard deviation was assessed and a t-test was performed to establish significance.

Vertical displacement measurements from all six beams is compared between LVDT and DIC and the results are summarised in Table 5. It can be seen that the ratio of DIC to LVDT data is very close to unity (1.04) and that the average standard deviation is much lower than for the strain measurement (0.028). For only one out of twelve cases is the difference in measurements from the two sensors significant (FRP1-b zone C). Compared to strain measurements, displacement measurements are less variable, leading to smaller measurement errors.

Table 5. Comparison of LVDT and DIC vertical deflection data

beam	C		FRP1-a		FRP1-b		FRP2		FRCM1		FRCM2		mean
zone	A	C	A	C	A	C	A	C	A	C	A	C	
ratio	1.07	1.16	1.01	1.02	0.98	1.13	0.99	0.96	0.97	0.97	1.06	1.15	1.04
s.d.	0.023	0.118	0.036	0.053	0.006	0.008	0.015	0.015	0.011	0.015	0.021	0.015	0.03
t-test	73%	9%	78%	67%	94%	2%	83%	56%	76%	55%	67%	7%	

Figure 7 illustrates the near perfect match in deflection data for beam FRP1-a in zone A as opposed to the less accurate data for beam FRCM2 in zone B. No significant difference can be attributed to the difference in surface material (concrete, FRP and FRCM) between the six

beams, highlighting that DIC is not dependent on the material surface as long as a high contrast pattern is identifiable.

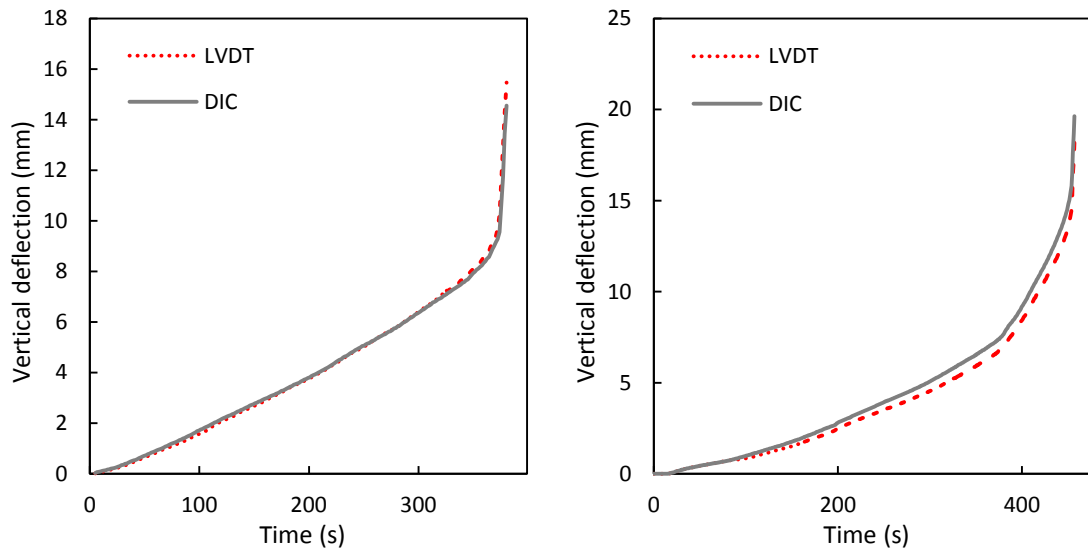


Figure 7 - Measured deflections in zone A for beam FRP1-a (left) and zone C for beam FRCM2 (right)

From these results it can be concluded that DIC is an adequate substitute for LVDT's, with the added advantage that it can give accurate values for displacement at any given point. Such monitoring hence allows the evolution of deflection across the length of the beam to be investigated as shown for half of the beam in Figure 9.

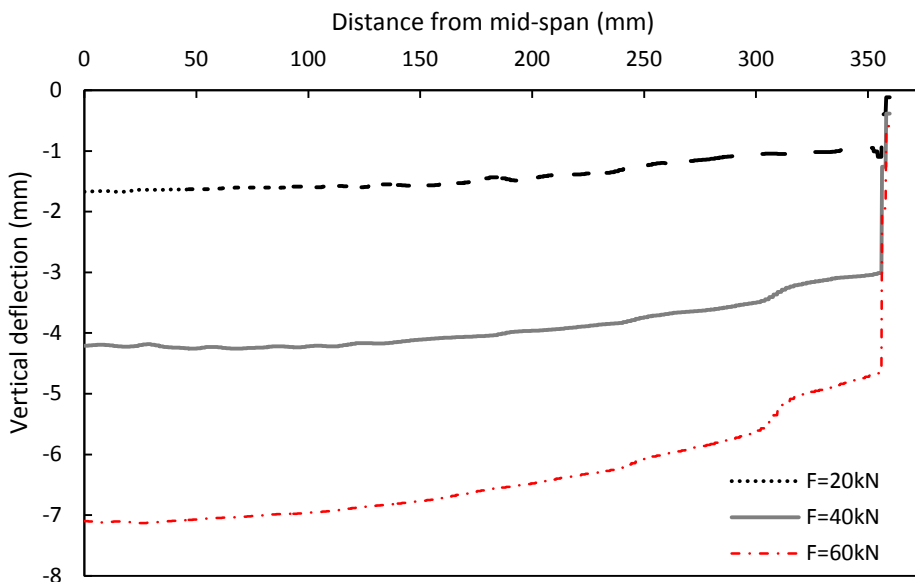


Figure 8 - Vertical deflection along one half of beam C measured using DIC

4.3. ACOUSTIC EMISSIONS

Finally, in order to monitor cracking and debonding throughout the tests, AE sensor data was analysed for four beam tests.

For the FRP-strengthened beams FRP1-b and FRP2, similarly to the FRP shear debonding tests, three clusters of frequency ranges were observed. These were labelled “concrete cracks” (100-175 kHz), “fibre-rupture” (250-400 kHz) and “FRP-debonding” (450-800Hz) in Figure 10, which shows the frequencies of the AE hits in comparison to the force-displacement plot of the beam. The cluster of frequencies attributed to debonding was observed at a lower frequency range then during the debonding tests. This can be associated to debonding happening cleanly at the FRP-epoxy-concrete interface for the debonding tests, while some concrete cover peels away with the FRP in the beam tests.

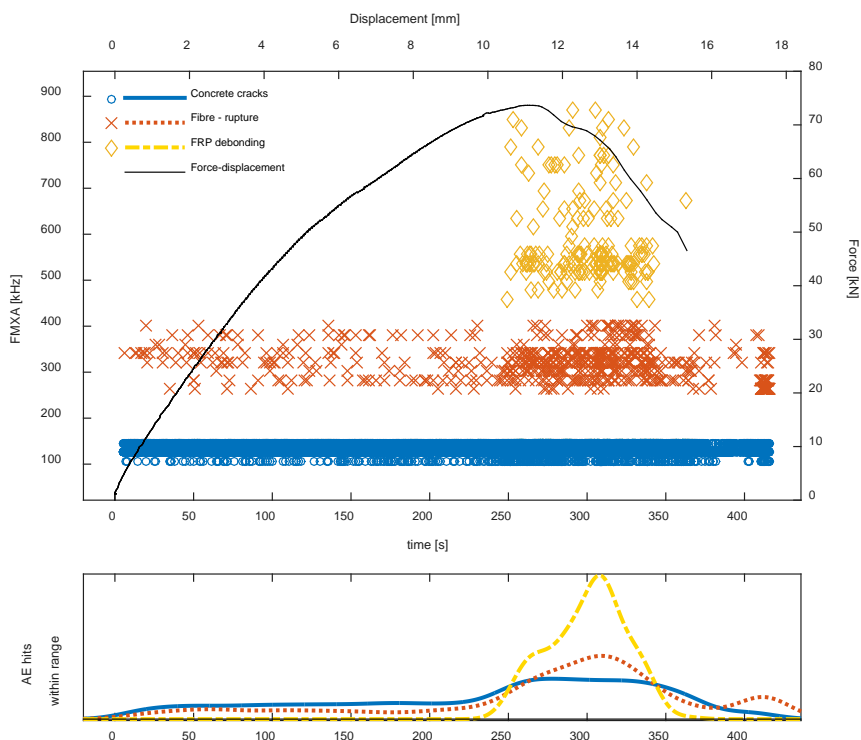


Figure 9 - Beam FRP1-b - top: transient frequencies of AE hits (FMXA) and Force-displacement plot; bottom: proportion of AE hits in range (not to scale)

Both FRP-strengthened beams fail in shear, with debonding of the FRP jackets starting in the lateral faces of the beam. As shown at the bottom of Figure 10, for beam FRP1-b, a steady increase in concrete cracks and low-amplitude FRP fracture events is observed initially. Shortly before the maximum load, around $t=250s$, failure of the beam is anticipated by an increase in rate of AE hits at these frequency ranges. This is also when AE signals with transient frequencies above 450 kHz are observed, coinciding with the observation of FRP debonding from the lateral faces of the beam. Very similar observations can be made for beam FRP2.

The Af/RA parametric analysis for FRP1-b is shown in Figure 10. When looking at the crack type analysis for both beams, a majority (85% and 95% for FRP1-b and FRP2 respectively) of cracks can be attributed to shear induced events. For the distribution of crack types within the three clusters of frequency ranges, it is observed that over 95% of events are shear related for the FRP-debonding frequencies, while over a quarter of cracks are tensile fractures in the lower FRP frequency cluster. This, in-turn, gives more confidence to the classification of FRP related frequency clusters.

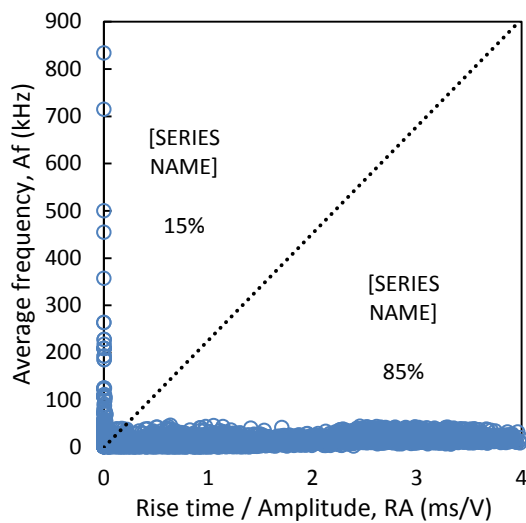


Figure 10 – Af/RA parameter analysis for beam FRP1-b

For the FRCM strengthened beams, two clusters of transient frequency ranges can be distinguished. The range of transient frequencies between 100 and 175 kHz, based on the material tests is attributed to concrete cracks. Although no material tests on FRCM were carried out, the range between 175 kHz and 250 kHz is attributed to FRCM events, e.g. mortar cracking

or fibre rupture, as this range of frequencies was not observed in any of the tests without FRCM.

For Beam FRCM1, as shown in Figure 11, the number of hits in both frequency ranges is increasing with force, as is the amplitude of hits. Before the yield point, a low increase in AE hits along with AE amplitudes below 60 dB are recorded. Changes in hit rate are observed at yield (around 6mm deflection), as well as at the peak force. Between yield and the peak force, the number of hits increases significantly and the amplitude of hits is at its highest, reaching up to 84.4 dB. The peak in acoustic emission hit count occurs just after the peak in force.

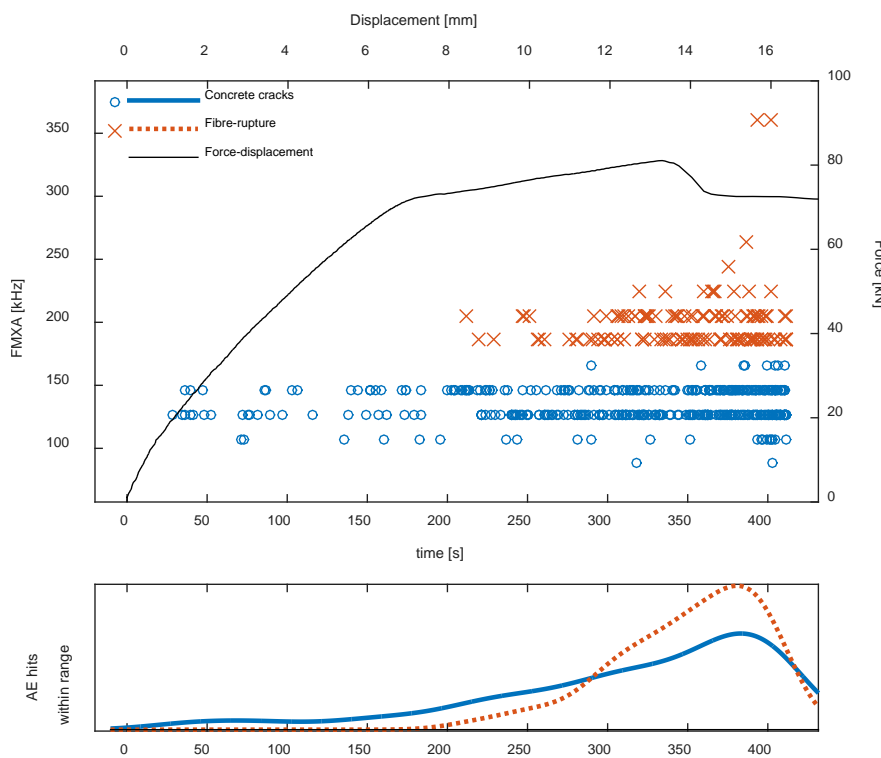


Figure 11 - Beam FRCM1 - top: transient frequencies of AE hits (FMXA) and Force-displacement plot; bottom: proportion of AE hits in range (not to scale)

Looking at the evolution of hits for the two frequency ranges separately, it is noted that in the first part of the plot, a steady increase in hits from concrete cracks is observed, while no hits in the FRCM frequency range were recorded. This compares well with observations during the test and the DIC analysis, as cracks on the FRCM surface were only noticed after $t=300s$. The rate of AE hits attributed to FRCM fracturing increases significantly around $t=275s$, hence before

observable cracks, and reaches a peak at $t=380s$, when a large flexural crack on the FRCM surface is observed.

The failure mechanism of beam FRCM1 is a combined shear and flexural failure, with a shear crack occurring on one side of the beam and flexural cracks opening around mid-span of the beam. The Af/RA analysis of the AE hits for beam FRCM1, shown in Figure 12, is in line with the observed failure mechanism, as 53% of hits are attributed to tensile cracks and 47% to shear movements. When analysing the Af/RA ratio for the two different frequency ranges, it is observed that for the concrete frequencies, about 51% shear cracks are recorded, while for the FRCM, for which more tensile cracks occurred, 65% of hits are classified as tensile. Moreover, when looking at the evolution of crack types with time, before yield, a majority of cracks are shear cracks, while close to the maximum load, the majority of cracks are tensile. Again, these trends are confirmed by experimental observations.

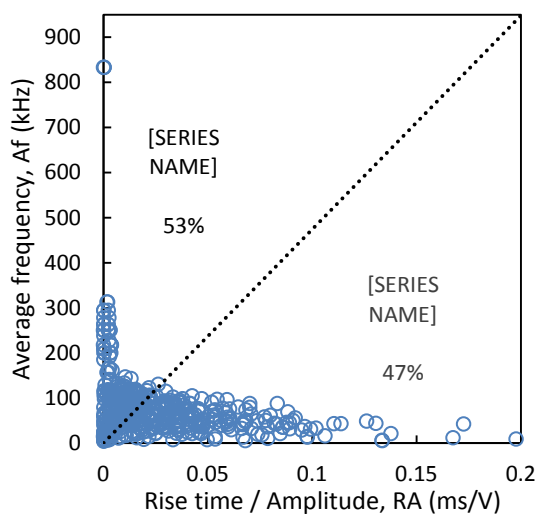


Figure 12 - Af/RA parameter analysis for beam FRCM1

For beam FRCM2, few cracks are observed on the FRCM jacket as the jacket debonds from the lateral faces. The beam fails due to a large shear crack on one side of the beam in the concrete below the FRCM jacket. Hits are only observed after one third of the experiment, possibly due to the thick FRCM jacket attenuating signals from concrete cracks below. Still, once hits were recorded, the large majority (95%) are observed in the frequency range of concrete cracks. This highlights a main benefit of using AE sensors, as cracks are only visibly observed towards the very end of the experiment. Again changes in hit count rate are seen at the yield point and the

maximum force. In terms of crack types, throughout the test, over 75% of hits are classified as shear movement cracks, which is confirmed by experimental observations. Unlike the FRP strengthened beams, the analysis of AE data does not provide any clear indication of the debonding of the FRCM jacket. This can be explained by the fact a rupture in a mortar-to-concrete bond likely produces similar AE waveforms to a concrete crack.

5. CONCLUSIONS

This paper offers a comparative analysis of different monitoring techniques for experiments on strengthened RC beams. It is shown that DIC gives accurate strain and displacement measurements in comparison to classical instrumentation. Compared to traditional methods, DIC has the advantage of not needing to apply instrumentation on the surface of the specimen, meaning there is no risk of affected measurements, as opposed to fibre-optics and strain gauges that can break and are affected by cracks. Latter also provide only local readings while DIC can give full-field data, as well as punctual measurements at different locations, using the virtual strain gauge in post-processing. Moreover, DIC can monitor strain and displacement simultaneously and can hence substitute LVDTs and strain gauges at the same time, making the preparation of experiments simpler. Still, a significant disadvantage of DIC is that it cannot measure deformations that occur below the surface of the retrofitting material or on the steel reinforcement. For these locations strain gauges or fibre-optics are necessary, particularly when debonding is expected. Between fibre-optics and strain gauges, some differences are observed in the presented experiments. These differences are mainly related to the application of the sensors and occurrence of cracks affecting the FBG sensors more. Strain gauges are cheaper and give more reliable results in the laboratory environment. For real structural health monitoring applications however, for instance in humid environments, fibre-optics have an advantage over strain gauges.

In order to detect damage within the specimen, even below the retrofitting material, AE sensors give accurate results. The rate of AE hit count is directly correlated with damage in the specimen and changes at yield and maximum force. This shows that AE can be used to anticipate failure of RC beams strengthened with composite materials. It is shown that different crack types and fracture mechanism are well characterised by analysing the A_f and RA parameters of AE recordings. By analysing the transient frequencies of the AE hits, the source

of AE hits in terms of material and fracture mechanism are also identified and this classification is confirmed from experimental observations. AE analysis gives more depth compared to simple observations as it can be used to identify and classify cracks below the surface of FRP and FRCM jackets, and hence before the visual observations and DIC analysis. Finally, FRP debonding is well characterised by AE analysis, however FCM debonding is not, and this can be explained by the nature of the debonding fracture mechanism.

Overall it can be concluded that the combined use of full-field NDT techniques such as DIC and AE proves very useful for the monitoring of strengthened beams. AE can accurately determine the onset and development of debonding, while DIC supplies quantitative information about the actual effective strain field on the entire specimen surface. These constitute two main parameters in design guidelines and AE and DIC are recommended for future experimental work in order to produce further empirical data to improve these.

6. ACKNOWLEDGMENTS

This research is part of the Challenging RISK project funded by EPSRC (EP/K022377/1). The authors acknowledge the staff of the Concrete Laboratory at UCL for the support during the experimental campaign. The CFRP and FRCM material used in this experimental campaign was kindly provided by S&P reinforcement. VMS Capture was kindly provided by Prof. Stuart Robson and LaVision provided an academic license for the DaVIS 8.3 software.

BIBLIOGRAPHY

- ACI 440, 2008. ACI 440.2R-08 - Guide for the design and construction of externally bonded FRP systems for strengthening concrete structures. American Concrete Institute, Farmington Hills, Mich.
- Akguzel, U., Pampanin, S., 2010. Seismic Upgrading of Exterior Beam-Column Joints Using GFRP. Presented at the 14th European Conference on Earthquake Engineering, Ohrid.
- Ali-Ahmad, M., Subramaniam, K., Ghosn, M., 2006. Experimental Investigation and Fracture Analysis of Debonding between Concrete and FRP Sheets. *J. Eng. Mech.* 132, 914–923. doi:10.1061/(ASCE)0733-9399(2006)132:9(914)
- Attari, N., Amziane, S., Chemrouk, M., 2012. Flexural strengthening of concrete beams using CFRP, GFRP and hybrid FRP sheets. *Constr. Build. Mater.* 37, 746–757. doi:10.1016/j.conbuildmat.2012.07.052
- Babaeidarabad, S., Loreto, G., Nanni, A., 2014. Flexural Strengthening of RC Beams with an Externally Bonded Fabric-Reinforced Cementitious Matrix. *J. Compos. Constr.* 18, 04014009. doi:10.1061/(ASCE)CC.1943-5614.0000473
- Barros, J.A.O., Dias, S.J.E., Lima, J.L.T., 2007. Efficacy of CFRP-based techniques for the flexural and shear strengthening of concrete beams. *Cem. Concr. Compos.* 29, 203–217. doi:10.1016/j.cemconcomp.2006.09.001

- Bisby, L.A., Stratford, T.J., 2011. The ultimate condition of FRP confined concrete columns: New experimental observations and insights, in: *Advances in FRP Composites in Civil Engineering*. Springer, pp. 599–602.
- Bousselham, A., 2010. State of Research on Seismic Retrofit of RC Beam-Column Joints with Externally Bonded FRP. *J. Compos. Constr.* 14, 49–61. doi:10.1061/(ASCE)CC.1943-5614.0000049
- CNR, 2012. DT 200.R1/2012 - Guide for the Design and Construction of Externally Bonded FRP Systems for Strengthening Existing Structures - Materials, RC and PC structures, masonry structures.
- Corr, D., Accardi, M., Graham-Brady, L., Shah, S., 2007. Digital image correlation analysis of interfacial debonding properties and fracture behavior in concrete. *Eng. Fract. Mech.* 74, 109–121. doi:10.1016/j.engfracmech.2006.01.035
- CSA, 2012. S806-12 - Design and construction of building structures with fibre-reinforced polymers.
- Degala, S., Rizzo, P., Ramanathan, K., Harries, K.A., 2009. Acoustic emission monitoring of CFRP reinforced concrete slabs. *Constr. Build. Mater.* 23, 2016–2026. doi:10.1016/j.conbuildmat.2008.08.026
- Del Vecchio, C., Di Ludovico, M., Balsamo, A., Prota, A., Manfredi, G., Dolce, M., 2014. Experimental Investigation of Exterior RC Beam-Column Joints Retrofitted with FRP Systems. *J. Compos. Constr.* 18. doi:10.1061/(ASCE)CC.1943-5614.0000459
- Dunegan, H., Harris, D., 1969. Acoustic emission-a new nondestructive testing tool. *Ultrasonics* 7, 160–166. doi:10.1016/0041-624X(69)90660-X
- El-Ghandour, A.A., 2011. Experimental and analytical investigation of CFRP flexural and shear strengthening efficiencies of RC beams. *Constr. Build. Mater.* 25, 1419–1429. doi:10.1016/j.conbuildmat.2010.09.001
- Esfahani, M.R., Kianoush, M.R., Tajari, A.R., 2007. Flexural behaviour of reinforced concrete beams strengthened by CFRP sheets. *Eng. Struct.* 29, 2428–2444. doi:10.1016/j.engstruct.2006.12.008
- fib (Ed.), 2001. fib Bulletin 14 - Externally bonded FRP reinforcement for RC structures: technical report on the design and use of externally bonded fibre reinforced polymer reinforcement (FRP EBR) for reinforced concrete structures. fib, Lausanne.
- Goidescu, C., Weleman, H., Garnier, C., Fazzini, M., Brault, R., Péronnet, E., Mistou, S., 2013. Damage investigation in CFRP composites using full-field measurement techniques: Combination of digital image stereo-correlation, infrared thermography and X-ray tomography. *Compos. Part B Eng.* 48, 95–105. doi:10.1016/j.compositesb.2012.11.016
- Grosse, C., Reinhardt, H., Finck, F., 2003. Signal-Based Acoustic Emission Techniques in Civil Engineering. *J. Mater. Civ. Eng.* 15, 274–279. doi:10.1061/(ASCE)0899-1561(2003)15:3(274)
- Gutkin, R., Green, C.J., Vangrattanachai, S., Pinho, S.T., Robinson, P., Curtis, P.T., 2011. On acoustic emission for failure investigation in CFRP: Pattern recognition and peak frequency analyses. *Mech. Syst. Signal Process.* 25, 1393–1407. doi:10.1016/j.ymsp.2010.11.014
- JCMS III, 2003. B5706k - Monitoring Method for Active Cracks in Concrete by Acoustic Emission. Federation of Construction Materials Industries Japan.
- Kaiser, H., Karbhari, V.M., 2004. Non-destructive testing techniques for FRP rehabilitated concrete. I: a critical review. *Int. J. Mater. Prod. Technol.* 21, 349–384.
- Kurtz, S., Balaguru, P., Helm, J., 2008. Experimental Study of Interfacial Shear Stresses in FRP-Strengthened RC Beams. *J. Compos. Constr.* 12, 312–322. doi:10.1061/(ASCE)1090-0268(2008)12:3(312)
- Lau, K., Yuan, L., Zhou, L., Wu, J., Woo, C., 2001. Strain monitoring in FRP laminates and concrete beams using FBG sensors. *Compos. Struct.* 51, 9–20. doi:10.1016/S0263-8223(00)00094-5
- Lee, J.-Y., Hwang, H.-B., Doh, J.-H., 2012. Effective strain of RC beams strengthened in shear with FRP. *Compos. Part B Eng.* 43, 754–765. doi:10.1016/j.compositesb.2011.11.050
- Lee, W.T., Chiou, Y.J., Shih, M.H., 2010. Reinforced concrete beam-column joint strengthened with carbon fiber reinforced polymer. *Compos. Struct.* 92, 48–60. doi:10.1016/j.compstruct.2009.06.011
- Lu, X.Z., Chen, J.F., Ye, L.P., Teng, J.G., Rotter, J.M., 2009. RC beams shear-strengthened with FRP: Stress distributions in the FRP reinforcement. *Constr. Build. Mater.* 23, 1544–1554. doi:10.1016/j.conbuildmat.2008.09.019

- Maji, A.K., Sahu, R., 1994. Acoustic emissions from reinforced concrete. *Exp. Mech.* 34, 379–388.
- Mazzotti, C., Savoia, M., Ferracuti, B., 2009. A new single-shear set-up for stable debonding of FRP–concrete joints. *Constr. Build. Mater., FRP Composites in Construction* 23, 1529–1537. doi:10.1016/j.conbuildmat.2008.04.003
- Ohno, K., Ohtsu, M., 2010. Crack classification in concrete based on acoustic emission. *Constr. Build. Mater., Special Issue on Fracture, Acoustic Emission and NDE in Concrete (KIFA-5)* 24, 2339–2346. doi:10.1016/j.conbuildmat.2010.05.004
- Ohtsu, M., 2008. Concrete, in: Grosse, C., Ohtsu, M. (Eds.), *Acoustic Emission Testing*. Springer Berlin Heidelberg, pp. 211–237.
- Pan, B., Xie, H., Wang, Z., Qian, K., Wang, Z., 2008. Study on subset size selection in digital image correlation for speckle patterns. *Opt. Express* 16, 7037. doi:10.1364/OE.16.007037
- Pohoryles, D.A., Rossetto, T., 2014. A critical evaluation of current design guidelines for the seismic retrofit of beam-column joints with FRP. Presented at the Second European Conference on Earthquake Engineering and Seismology, Istanbul, Turkey.
- Sayed, A.M., Wang, X., Wu, Z., 2014. Evaluation of effective strain of FRP sheets for shear strengthened RC beams. Presented at the The 7th International Conference on FRP Composites in Civil Engineering, Vancouver, Canada.
- Shahidan, S., Pulin, R., Muhamad Bunnori, N., Holford, K.M., 2013. Damage classification in reinforced concrete beam by acoustic emission signal analysis. *Constr. Build. Mater.* 45, 78–86. doi:10.1016/j.conbuildmat.2013.03.095
- Teo, W., Yin, H., 2014. Optimized effective strain model for externally bonded FRP shear strengthened RC members. Presented at the The 7th International Conference on FRP Composites in Civil Engineering, Vancouver, Canada.
- Verbruggen, S., Aggelis, D.G., Tysmans, T., Wastiels, J., 2014. Bending of beams externally reinforced with TRC and CFRP monitored by DIC and AE. *Compos. Struct.* 112, 113–121. doi:10.1016/j.compstruct.2014.02.006
- Wevers, M., 1997. Listening to the sound of materials: Acoustic emission for the analysis of material behaviour. *NDT E Int.* 30, 99–106. doi:10.1016/S0963-8695(96)00051-5
- Zhang, B., Benmokrane, B., Nicole, J.-F., 2003. Laboratory Evaluation of Fiber-Optic Sensors for Strain Monitoring. *J. Mater. Civ. Eng.* 15, 381–390. doi:10.1061/(ASCE)0899-1561(2003)15:4(381)